Enhanced coherent Thomson scattering in the few-cycle regime

KE HU[1] AND HUI-CHUN WU[1,2,*]

[1] Institute for Fusion Theory and Simulation (IFTS) and Department of Physics, Zhejiang University, Hangzhou 310027, China
[2] IFSA Collaborative Innovation Center, Shanghai Jiao Tong University, Shanghai 200240, China
[*] Corresponding author: huichunwu@zju.edu.cn

Compiled April 23, 2016

We study x-ray production by coherent nonlinear Thomson scattering of few-cycle laser pulses from relativistic electron sheets. For an electron sheet thicker than the wavelength of the x-ray, the scattering efficiency is found to increase by two orders of magnitude for single-cycle laser pulses as compared with longer pulses. This enhancement is attributed to suppression of destructive interference during the scattering process, as well as frequency downshift related to the ultrabroad spectra of single-cycle pulses. The x-ray amplitude in this nonadiabatic regime is calculated and agrees with that from particle-in-cell simulation. These results can be useful for designing more intense, shorter attosecond x-ray sources.

OCIS codes: *(320.7110) Ultrafast nonlinear optics; (340.7480) X-rays, soft x-rays, extreme ultraviolet (EUV); (290.1350) Backscattering; (350.5720) Relativity.*

http://dx.doi.org/10.1364/ao.XX.XXXXXX

Coherent x-ray sources, such as the free electron laser [1] and high harmonic generation (HHG) from laser interaction with gas targets [2], are opening new regimes of nonlinear x-ray optics [3] and attosecond science [4]. The free-electron laser can produce >10GW femtosecond x-ray pulses. HHG from gas targets can generate attosecond XUV pulses at low photon flux. Some relativistic laser-plasma processes can deliver attosecond pulses as powerful as that from free-electron lasers and shorter than that from gas targets. These processes include HHG from laser-irradiated solid surfaces [5–7], coherent Thomson scattering [8, 9] and half-cycle-wave emission from relativistic electron sheets [10, 11]. These novel sources are useful for attosecond diagnostics and understanding/investigating nonlinear attosecond physics [12, 13].

Coherent Thomson scattering from relativistic electron sheets can potentially produce >10GW and <10as isolated x-ray pulses [9]. These electron sheets are formed by laser-accelerated electrons from nano-foils [8, 14] or laser-driven plasma waves [15, 16] in underdense plasmas. Consider an electron sheet with the relativistic factor $\gamma = 1/\sqrt{1-(V/c)^2}$, where V is the electron velocity normal to the sheet plane. When a second, counter-propagating, laser pulse is reflected from the sheet, its frequency is Doppler upshifted by $4\gamma^2$. Thus, x-rays can be produced at the modest electron energy of tens of MeV.

In earlier works the scattering efficiency has been analyzed for flat-top or long-pulse lasers [9, 17], and is independent of the pulse duration. In this paper, we study coherent Thomson scattering in the few-cycle regime, and found that the conversion efficiency can be significantly increased. The scattering enhancement is attributed to suppression of destructive interference and frequency downshift of the scattered signal. This finding can circumvent the problem of weakening scattering from thicker sheets as a result of the destructive scattering, as pointed out in Ref. [9]. The field amplitude, the enhancement condition, and the frequency downshift of the scattered x-rays are obtained analytically, and confirmed by particle-in-cell (PIC) simulation.

To calculate the peak amplitude of the scattered x-rays, we first transform the equations and parameters to the rest frame of the electron sheet riding at the laser peak, derive the scattering amplitude, and then transform it back to the lab frame. Assume the electron sheet has a density profile $n_e(x) = n_0 \exp(-\pi x^2/d_0^2)$, where n_0 and d_0 are the peak density and characteristic thickness, respectively. The sheet is in the yz plane and moves along the x axis with a normalized momentum $p_0 = P_0/mc$ and relativistic factor $\gamma_0 = \sqrt{1+p_0^2}$, where m is the electron mass and c is the light speed. The laser pulse is circularly-polarized and its vector potential is $\mathbf{a}(\zeta) = e\mathbf{A}/mc = a_0 f(\zeta) \times [\hat{y}\cos(\omega_0\zeta) + \hat{z}\sin(\omega_0\zeta)]$, where $a_0 = eA_0/mc$, $f(\zeta) = \exp[-(\zeta/T)^2]$, $\omega_0 = 2\pi/\tau_0$, $\zeta = t + x/c$, T is the pulse duration, and $\tau_0 = \lambda_0/c$ is the light wave cycle.

Coulomb expansion of the electron sheet and radiation reaction is negligible within the present ultrashort scattering process. The sheets produced from the laser-driven nanofoils have a typical energy spread of $\sim 0.1\%$ [8, 9] and are assumed to be monoenergetic. The electron motion in the head-on relativistic laser pulse is completely determined by the laser field. For an electron with the initial perpendicular and parallel momenta

$\mathbf{p}_{\perp 0} = 0$ and $p_{x0} = p_0$, respectively, we have [9]

$$\begin{aligned} \mathbf{p}_\perp(\zeta) &= \mathbf{a}(\zeta), \\ p_x(\zeta) &= \frac{(\gamma_0+p_0)^2 - [1+a(\zeta)^2]}{2(\gamma_0+p_0)}, \\ \gamma(\zeta) &= \frac{(\gamma_0+p_0)^2 + [1+a(\zeta)^2]}{2(\gamma_0+p_0)}. \end{aligned} \tag{1}$$

When the sheet center coincides with the maximum laser field a_0, the longitudinal velocity of an electron there has

$$\beta_x|_{a_0} = \frac{p_x|_{a_0}}{\gamma|_{a_0}} = \frac{(\gamma_0+p_0)^2 - (1+a_0^2)}{(\gamma_0+p_0)^2 + (1+a_0^2)}. \tag{2}$$

The wavelength of produced x-rays is then given by $\lambda_{cts} = \lambda_0/D$, where $D = (1+\beta_x|_{a_0})/(1-\beta_x|_{a_0}) \approx 4\gamma^2/(1+a_0^2)$ is the Doppler factor in the relativistic laser and a_0^2 describes the nonlinearity.

We perform a Lorentz transformation from the lab frame to a boosted frame moving with $\beta_x|_{a_0}$ along the x axis. In the new frame, the initial relativistic factor and velocity of the electrons are $\gamma_0' = (1+a_0^2/2)/\sqrt{1+a_0^2}$ and $\beta_0' = a_0^2/(2+a_0^2)$, respectively. Since the vector potential $\mathbf{a}(\zeta)$ is a Lorentz invariant, similar to Eq. (1) in the lab frame, the electron motion is given by

$$\begin{aligned} \mathbf{p}_\perp'(\zeta') &= \mathbf{a}(\zeta'), \\ p_x'(\zeta') &= \frac{a_0^2 - a_0^2 f(\zeta')^2}{2\sqrt{1+a_0^2}}, \\ \gamma'(\zeta') &= \frac{2+a_0^2+a_0^2 f(\zeta')^2}{2\sqrt{1+a_0^2}}. \end{aligned} \tag{3}$$

In the flat-top ($f = 1$) laser pulse [9], all electrons remain stationary in the longitudinal direction, i.e. $p_x' = 0$. However, for a few-cycle pulse, the effect of the varying envelope $f(\zeta')$ in Eq. (3) must be considered, and only electrons at the sheet center have $p_x'(\zeta' = 0) = 0$.

In the boosted frame, the laser pulse can compress the electron sheet longitudinally. From Eq. (3), the electron velocity in the x direction is

$$\beta_x'(\zeta') = \frac{p_x'(\zeta')}{\gamma'(\zeta')} = \frac{a_0^2 - a_0^2 f(\zeta')^2}{2+a_0^2+a_0^2 f(\zeta')^2}. \tag{4}$$

We consider two electrons with initial positions x_{1i}' and x_{2i}', and let the first electron meet the laser front at $t' = 0$. At t', these two electrons reach the positions x_{1f}' and x_{2f}', corresponding to ζ_1' and ζ_2' within the laser envelope, respectively. Accordingly, we have

$$t' = \int_0^{\zeta_1'} \frac{d\zeta''}{1+\beta_x'(\zeta'')}, \tag{5}$$

$$t' - \frac{x_{1i}' - x_{2i}'}{c(1+\beta_0')} = \int_0^{\zeta_2'} \frac{d\zeta''}{1+\beta_x'(\zeta'')}, \tag{6}$$

where $(x_{1i}' - x_{2i}')/[c(1+\beta_0')]$ is the time interval for the laser to propagate from the first electron to the second one. When the initial spacing $x_{1i}' - x_{2i}' \ll \lambda'$, substituting Eq. (5) into Eq. (6), we obtain

$$\frac{x_{1i}' - x_{2i}'}{c(1+\beta_0')} = \int_{\zeta_2'}^{\zeta_1'} \frac{d\zeta''}{1+\beta_x'(\zeta'')} \simeq \frac{\zeta_1' - \zeta_2'}{1+\beta_x'(\zeta')}, \tag{7}$$

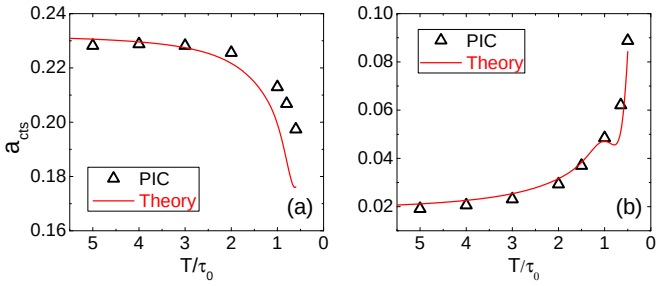

Fig. 1. Peak amplitude a_{cts} of the scattered x-rays vs. laser duration T for $a_0 = 5$ (a) and $a_0 = 3.5$ (b).

so that we have the compression ratio

$$\eta'(\zeta') = \frac{x_{1i}' - x_{2i}'}{x_{1f}' - x_{2f}'} = \frac{x_{1i}' - x_{2i}'}{c(\zeta_1' - \zeta_2')} = \frac{1+\beta_0'}{1+\beta_x'(\zeta')}. \tag{8}$$

After this drift compression, the sheet density becomes

$$n_e'|_{a_0}(x', \zeta') = n'|_{a_0}(\zeta') \exp\left[\frac{-\pi x'^2}{d'|_{a_0}(\zeta')^2}\right], \tag{9}$$

where $n'|_{a_0}(\zeta') = n_0'\eta'(\zeta') = (\gamma_0'/\gamma_0)n_0\eta'(\zeta')$ and $d'|_{a_0}(\zeta') = d_0'/\eta'(\zeta') = (\gamma_0/\gamma_0')d_0/\eta'(\zeta')$. Here the density profile deviates slightly from the simple gaussian distribution due to the appearance of ζ' in Eq. (9).

The scattered electromagnetic amplitude can be obtained from the wave equation $(\partial^2/\partial x'^2 - c^{-2}\partial^2/\partial t'^2)\mathbf{A}_{cts}' = -\mu_0 \mathbf{J}'(x', t')$, where $\mathbf{J}'(x', t') = -ecn_e'|_{a_0}(x' - x'|_{a_0}, \zeta')\mathbf{p}_\perp'(\zeta')/\gamma'(\zeta')$ is the current density, and $x'|_{a_0}$ is the electron position at the sheet center. The scattered signal has the electric field

$$\mathbf{E}_{cts}' = -\frac{\partial}{\partial t'}\left[\frac{c\mu_0}{2}\int_{-\infty}^{\infty} dx'' \int_{-\infty}^{t' - \frac{|x'-x''|}{c}} \mathbf{J}'(x'', t'')dt''\right]. \tag{10}$$

We numerically integrate Eq. (10) to obtain the peak amplitude, and transform it back to the lab frame through $\mathbf{E}_{cts} = \mathbf{E}_{cts}'\sqrt{(1+\beta_x|_{a_0})/(1-\beta_x|_{a_0})}$.

We simulate coherent Thomson scattering of few-cycle laser pulses by the code JPIC [18], which adopts the boosted PIC technique [9] for ultrafast and high-precision computation. The electron sheet has $d_0 = 0.6$nm, $n_0 = 10n_c$ and $\gamma_0 = 70$, where $n_c = \varepsilon_0 m\omega_0^2/e^2$ is the critical density. The laser pulse has $\lambda_0 = 800$nm. Since the definition of pulse envelope becomes invalid for $T < 0.5\tau_0$ [19], for the shortest pulse we take $T_{min} = 0.5\tau_0$.

Figure 1(a) shows the x-ray amplitude a_{cts} versus the pulse duration T for $a_0 = 5$ and 3.5. We see that the PIC results confirm that from our theory. At $T = 5\tau_0$, the results agree with that of the long-pulse theory of Ref. [9]. For $a_0 = 5$, the scattered signal first remains constant, and then decreases slightly for $T < 3\tau_0$. In contrast, at $a_0 = 3.5$, the amplitude increases dramatically when the pulse duration is shortened to $0.5\tau_0$.

The evolution of a_{cts} with T in Fig. 1 can be interpreted in terms of the interference effect of coherent scattering. The x-ray amplitude a_{cts} is proportional to the space-time integral of the current density J' in Eq. (10). Figure 2 shows the density profiles of the electron sheets calculated from Eq. (9) and the laser vector potentials a_y' when the sheet center coincides with the laser peak. The vertical dashed lines indicate the positions of two nodes of a_y' around the sheets. According to Eq. (3), a_y' is the same as the transverse momentum of electrons.

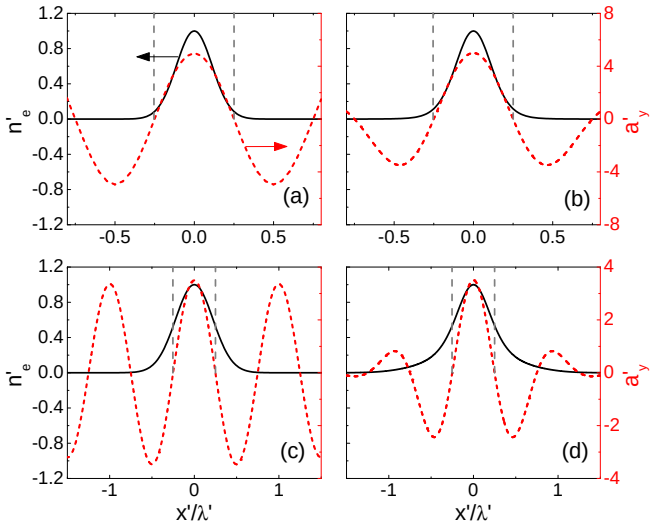

Fig. 2. Electron sheet density n'_e (solid curve) and laser vector potential a'_y (dashed curve) for $a_0 = 5$ (a,b) and $a_0 = 3.5$ (c,d). Pulse duration T is $5\tau_0$ in (a,c) and $0.8\tau_0$ in (b,d). Vertical dashed lines mark the nodes of the vector potentials.

As illustrated in Fig. 2(a) and Fig. 2(b), for $a_0 = 5$, almost all of electrons in the sheet are located inside the positive-momentum region between the dashed lines for both $T = 5$ and $0.8\tau_0$. This accounts for the weak dependence of the scattering amplitude on the pulse duration shown in Fig. 1(a). The slight amplitude decrease is due to the smaller compression ratio η' in Eq. (8) at $T = 0.8\tau_0$. This causes some electrons in the sheet wings to slide into the negative-momentum region (see Fig. 2(b)), which results in a small reduction of the radiation emitting from the positive-momentum region.

For $a_0 = 3.5$, a large portion of the electrons in the sheet are already in the negative-momentum region. As the pulse duration T decreases from $5\tau_0$ to $0.8\tau_0$, the amplitudes of the two negative antinodes of the laser field are considerably decreased (see Fig. 2(d)). Therefore, the destructive interference in the radiating process is significantly mitigated, which is responsible for the dramatic scattering enhancement shown in Fig. 1(b). The amplitude a_{cts} at $T = 0.5\tau_0$ is 4.6 times that produced at $T = 5\tau_0$, i.e., a 21-fold increase in the peak power.

From the theory, we find that the scattering enhancement occurs at $d'_0|_{a_0}/\lambda' \geqslant 0.45$, where $d'_0|_{a_0} = d'|_{a_0}(\zeta' = 0)$ is the sheet thickness at the laser peak. Tranforming back to the lab frame, we obtain

$$d_0 \geqslant 0.45\frac{\lambda_0(1+a_0^2)}{\gamma_0^2(1+\beta_0)} \simeq 0.9\lambda_{cts}. \qquad \textbf{(11)}$$

Therefore, when the electron sheet is thicker than the wavelength of the produced x-rays, the coherent scattering can be considerably enhanced by using a single-cycle laser pulse. We note that for $a_0 = 3.5$ and 5 (Fig. 1), one has $d_0 \approx 1.1\lambda_{cts}$ and $d_0 \approx 0.56\lambda_{cts}$, respectively.

In the long-pulse case, the x-ray signal has the central frequency $\omega_{cts} = \omega_0 D$, independent of the pulse duration. However, we find that the central frequency becomes dependent on T in the few-cycle regime. Figure 3(a) shows that $\omega_{cts}/(\omega_0 D)$ monotonically decreases with T for both $a_0 = 5$ and 3.5.

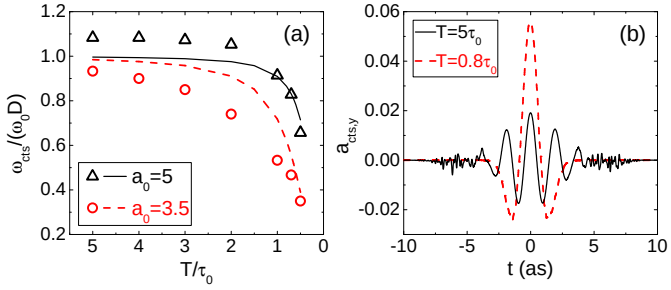

Fig. 3. (a) Central frequency ω_{cts} of scattered x-rays vs. pulse duration T for $a_0 = 5$ and 3.5. Open triangles and circles: PIC results, solid and dashed curves: from Eq. (12). (b) Electric field profile $a_{cts,y}$ of scattered x-rays for $a_0 = 3.5$.

To quantitatively calculate the frequency downshift, we again consider the scattering process in the boosted frame. For the gaussian pulse $f(\zeta') = \exp[-(\zeta'/T')^2]$, its spectral amplitude is given by $F(\omega') \propto \exp[-(\omega' - \omega'_0)T'^2/4]$. For each component at the frequency ω', the scattering amplitude is proportional to $\exp[-4\pi(d'_0|_{a_0}/\lambda')^2]$ [9], where $\lambda' = 2\pi\omega'/c$. Here, we adopt the constant sheet thickness $d'_0|_{a_0}$ at the laser peak. Then, the spectral amplitude of the scattered signal scales with $\exp[-(\omega' - \omega'_0)T'^2/4 - 4\pi(d'_0|_{a_0}/\lambda')^2]$, which is maximum at the central frequency $\omega'_{cts}/\omega'_0 = \pi(T'/\tau'_0)^2/[\pi(T'/\tau'_0)^2 + 4(d'_0|_{a_0}/\lambda'_0)^2]$. Transforming back to the lab frame, we obtain

$$\omega_{cts} = \omega_0 D\frac{\pi(T/\tau_0)^2}{\pi(T/\tau_0)^2 + (d_0/\lambda_{cts})^2}. \qquad \textbf{(12)}$$

For a long pulse with $T \gg \tau_0$ or an ideal delta-function density profile ($d_0 \to 0$), Eq. (12) leads to the well known relation $\omega_{cts} = \omega_0 D$. Similar to the amplitude enhancement discussed above, Eq. (12) indicates that the frequency downshift only occurs when $d_0 \sim \lambda_{cts}$.

In Fig. 3(a), Eq. (12) can reasonably reproduce the trend observed in the PIC simulations and thus be used for rough estimations. The discrepancy mainly comes from the approximation of constant thickness $d'_0|_{a_0}$. We have verified that Eq. (12) agrees precisely with the PIC results in the low-intensity regime $a_0^2 \ll 1$. Figure 3(b) shows the electric fields of the scattered x-rays for $a_0 = 3.5$. It is obvious that the x-ray wavelength at $T = 0.8\tau_0$ is longer than that at $T = 5\tau_0$. The x-ray pulse is shorter than 10as and has a peak intensity $1.3 \times 10^{16}\mathrm{W/cm^2}$ at $T = 0.8\tau_0$. For an emission spot of 5μm in radius, the peak power can reach 10GW.

Now, we discuss the efficiency of energy conversion from laser to x-ray. As shown in Fig. 4(a), for $a_0 = 5$, the efficiency increases by about 46% when $T \to 0.5\tau_0$, although the peak amplitude a_{cts} decreases with T (see Fig. 1(a)). This can be attributed to the frequency downshift appearing in Fig. 3(a). If the signal contains the same number of light cycles, it will be elongated due to the frequency downshift. For $a_0 = 3.5$ in Fig. 4(b), amplitude enhancement together with frequency downshift boost the efficiency by more than two orders of magnitude. Above all, for a realistic electron sheet (finite thickness), one can utilize a single-cycle pulse to enhance the x-ray generation. Finally, we stress that the nonadiabatic effects in Eq. (11) and Eq. (12) also apply for the linear case $a_0^2 \ll 1$.

In conclusion, we have found two nonadiabatic phenomena of nonlinear coherent Thomson scattering in the few-cycle regime: amplitude enhancement and frequency downshift. The

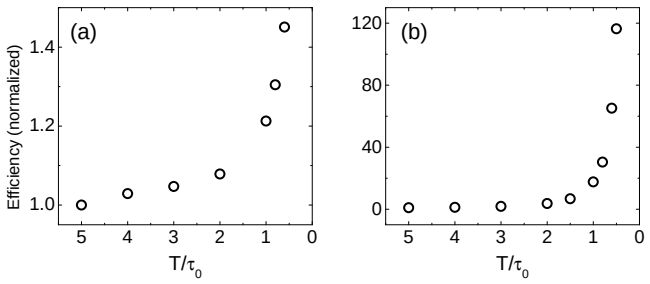

Fig. 4. Scattering efficiency (normalized to the values at $T = 5\tau_0$) vs. pulse duration T for $a_0 = 5$ (a) and $a_0 = 3.5$ (b).

former is caused by mitigation of destructive interference in the scattering process and the latter is due to the optimum frequency selection from the ultrabroad spectra of the few-cycle pulses. These nonadiabatic effects can boost the scattering efficiency by more than one hundred times, when the electron sheet is thicker than the wavelength of produced x-rays. These findings can be useful for developing more intense, shorter attosecond x-ray sources based on relativistic electron sheets.

FUNDING.

The Thousand Youth Talents Plan, NSFC (11374262); Fundamental Research Funds for the Central Universities.

ACKNOWLEDGEMENT.

The authors thank M. Y. Yu for helpful comments.

REFERENCES

1. B. W. J. McNeil and N. R. Thompson, Nat. Photon. **4**, 814 (2010).
2. C. Winterfeldt, C. Spielmann, and G. Gerber, Rev. Mod. Phys. **80**, 117 (2008).
3. K. Tamasaku, E. Shigemasa, Y. Inubushi, T. Katayama, K. Sawada, H. Yumoto, H. Ohashi, H. Mimura, M. Yabashi, K. Yamauchi, and T. Ishikawa, Nat. Photon. **8**, 313 (2014).
4. F. Krausz and M. Ivanov, Rev. Mod. Phys. **81**, 163 (2009).
5. R. Lichters, J. Meyer-ter-Vehn, and A. Pukhov, Phys. Plasmas **3**, 3425 (1996).
6. T. Baeva, S. Gordienko, and A. Pukhov, Phys. Rev. E **74**, 065401 (2006).
7. U. Teubner and P. Gibbon, Rev. Mod. Phys. **81**, 445 (2009).
8. H.-C. Wu, J. Meyer-ter-Vehn, J. Fernández, and B. M. Hegelich, Phys. Rev. Lett. **104**, 234801 (2010).
9. H.-C. Wu, J. Meyer-ter-Vehn, B. M. Hegelich, and J. C. Fernández, Phys. Rev. ST Accel. Beams **14**, 070702 (2011).
10. H.-C. Wu and J. Meyer-ter-Vehn, Nat. Photon. **6**, 304 (2012).
11. F. Y. Li, Z. M. Sheng, M. Chen, L. L. Yu, J. Meyer-ter-Vehn, W. B. Mori, and J. Zhang, Phys. Rev. E **90**, 043104 (2014).
12. G. Sansone, L. Poletto, and M. Nisoli, Nat. Photon. 5, 655 (2011).
13. A. Nazarkin, Phys. Rev. Lett. **97**, 163904 (2006).
14. V. V. Kulagin, V. A. Cherepenin, M. S. Hur, and H. Suk, Phys. Rev. Lett. **99**, 124801 (2007).
15. S.V. Bulanov, T. Zh. Esirkepov, and T. Tajima, Phys. Rev. Lett. **91**, 085001 (2003).
16. F. Y. Li, Z. M. Sheng, Y. Liu, J. Meyer-ter-Vehn, W. B. Mori, W. Lu, and J. Zhang, Phys. Rev. Lett. **110**, 135002 (2013).
17. H.-C. Wu and J. Meyer-ter-Vehn, Eur. Phys. J. D **55**, 443 (2009).
18. H.-C. Wu, http://arxiv.org/abs/1104.3163.
19. T. Brabec and F. Krausz, Phys. Rev. Lett. **78**, 3282 (1997).

REFERENCES

1. B. W. J. McNeil and N. R. Thompson, "X-ray free-electron lasers," Nat. Photon. **4**, 814 (2010).
2. C. Winterfeldt, C. Spielmann, and G. Gerber, "Colloquium: Optimal control of high-harmonic generation," Rev. Mod. Phys. **80**, 117 (2008).
3. K. Tamasaku, E. Shigemasa, Y. Inubushi, T. Katayama, K. Sawada, H. Yumoto, H. Ohashi, H. Mimura, M. Yabashi, K. Yamauchi, and T. Ishikawa, "X-ray two-photon absorption competing against single and sequential multiphoton processes," Nat. Photon. **8**, 313 (2014).
4. F. Krausz and M. Ivanov, "Attosecond physics, " Rev. Mod. Phys. **81**, 163 (2009).
5. R. Lichters, J. Meyer-ter-Vehn, and A. Pukhov, "Short-pulse laser harmonics from oscillating plasma surfaces driven at relativistic intensity," Phys. Plasmas **3**, 3425 (1996).
6. T. Baeva, S. Gordienko, and A. Pukhov, "Theory of high-order harmonic generation in relativistic laser interaction with overdense plasma," Phys. Rev. E **74**, 065401 (2006).
7. U. Teubner and P. Gibbon, "High-order harmonics from laser-irradiated plasma surfaces," Rev. Mod. Phys. **81**, 445 (2009).
8. H.-C. Wu, J. Meyer-ter-Vehn, J. Fernández, and B. M. Hegelich, "Uniform Laser-Driven Relativistic Electron Layer for Coherent Thomson Scattering," Phys. Rev. Lett. **104**, 234801 (2010).
9. H.-C. Wu, J. Meyer-ter-Vehn, B. M. Hegelich, and J. C. Fernández, "Nonlinear coherent Thomson scattering from relativistic electron sheets as a means to produce isolated ultrabright attosecond x-ray pulses," Phys. Rev. ST Accel. Beams **14**, 070702 (2011).
10. H.-C. Wu and J. Meyer-ter-Vehn, "Giant half-cycle attosecond pulses," Nat. Photon. **6**, 304 (2012).
11. F. Y. Li, Z. M. Sheng, M. Chen, L. L. Yu, J. Meyer-ter-Vehn, W. B. Mori, and J. Zhang, "Radially polarized, half-cycle, attosecond pulses from laser wakefields through coherent synchrotronlike radiation," Phys. Rev. E **90**, 043104 (2014).
12. G. Sansone, L. Poletto, and M. Nisoli, "High-energy attosecond light sources," Nat. Photon. 5, 655 (2011).
13. A. Nazarkin, "Nonlinear Optics of Intense Attosecond Light Pulses," Phys. Rev. Lett. **97**, 163904 (2006).
14. V. V. Kulagin, V. A. Cherepenin, M. S. Hur, and H. Suk, "Theoretical Investigation of Controlled Generation of a Dense Attosecond Relativistic Electron Bunch from the Interaction of an Ultrashort Laser Pulse with a Nanofilm," Phys. Rev. Lett. **99**, 124801 (2007).
15. S.V. Bulanov, T. Zh. Esirkepov, and T. Tajima, "Light Intensification towards the Schwinger Limit," Phys. Rev. Lett. **91**, 085001 (2003).
16. F. Y. Li, Z. M. Sheng, Y. Liu, J. Meyer-ter-Vehn, W. B. Mori, W. Lu, and J. Zhang, "Dense Attosecond Electron Sheets from Laser Wakefields Using an Up-Ramp Density Transition," Phys. Rev. Lett. **110**, 135002 (2013).
17. H.-C. Wu and J. Meyer-ter-Vehn, "The reflectivity of relativistic ultra-thin electron layers," Eur. Phys. J. D **55**, 443 (2009).
18. H.-C. Wu, "JPIC & How to make a PIC code," http://arxiv.org/abs/1104.3163.
19. T. Brabec and F. Krausz, "Nonlinear optical pulse propagation in the single-cycle regime," Phys. Rev. Lett. **78**, 3282 (1997).